Spatial Transformations of High Angular Resolution Diffusion Imaging Data in Q-space

Thijs Dhollander[1,2], Wim Van Hecke[1,3,4], Frederik Maes[1,2], Stefan Sunaert[1,3], and Paul Suetens[1,2]

[1] Medical Imaging Research Center (MIRC), K.U.Leuven, Leuven, Belgium
[2] Center for Processing Speech and Images (PSI), Department of Electrical Engineering (ESAT), Faculty of Engineering, K.U.Leuven, Leuven, Belgium
[3] Department of Radiology, University Hospitals of the K.U.Leuven, Leuven, Belgium
[4] Department of Radiology, University Hospital Antwerp, Antwerp, Belgium

Abstract. A crucial operation in every image registration algorithm is the application of a spatial transformation to an image. For scalar valued images, this particular operation is rather trivial. For diffusion weighted imaging (DWI) data however, the problem is more complex due to the information in every voxel being dependent on the angular structure of the underlying tissue. Methods for transforming the diffusion tensor and the fiber orientation distribution function from high angular resolution diffusion imaging have already been proposed. In order to perform registration of DWI data irrespectively of (i.e. *before* the application of) any particular reconstruction method, it should be done straight on the signal functions in q-space. In this work, we specifically consider the problem of transforming the signal functions in q-space. We develop a plausible method to accomplish this. The proposed method preserves anisotropic as well as isotropic volume fractions.

1 Introduction

Diffusion weighted imaging (DWI) is a magnetic resonance imaging (MRI) technique that allows to study the oriented microstructure of tissue in vivo through the assessment of the self-diffusion of water within this tissue. In high angular resolution diffusion imaging (HARDI), many volumes are acquired using different gradient directions. From these data, higher order reconstructions can be made, including, but not limited to the apparent diffusion coefficient (ADC) profile [1, 5], the diffusion orientation distribution function (dODF) from Q-Ball imaging (QBI) [2, 6] and the fiber orientation distribution function (fODF) from spherical deconvolution (SD) of the data [3, 4] or the dODF [7]. An advantage of higher order models is the ability to represent more complex fiber structures, where the diffusion tensor (DT) obtained from diffusion tensor imaging (DTI) is unable to do so. The methods of Descoteaux et al. [5–7] are notable because they yield simple relations between the signals in q-space, the dODF and the fODF using a symmetric, real, orthonormal spherical harmonics (SH) basis.

The application of a spatial transformation is a crucial operation in any registration / normalization algorithm. For DWI data or any of the previously

mentioned reconstructions, this is a challenge of its own since the information in every voxel is angularly dependent on the microstructure of the underlying tissue. In the case of a non-rigid deformation field, the Jacobian matrix can be calculated at the position of each voxel. This provides a local affine model, and as such reduces the problem to *affine transformation of the information in a single voxel*.

For DTI, it has been argued that the DT should only undergo a rigid rotation so as to preserve the properties of the tissue [8]. Through strategies such as finite strain (FS) or preservation of principal direction (PPD), the rigid rotation matrix can be obtained. Barmpoutis et al. [9] represent diffusion by a 4^{th} order tensor and show how this can be affinely transformed. Both Hong et al. [12] and Raffelt et al. [13] tackle the problem of transforming the fODF. Their assumption of the final result is the same: applying the affine transformation to the directions while preserving the volume fractions of the fiber populations (this is reasonable, as the fODF is a probability distribution function). Although their methods to accomplish this goal are different, similar results should theoretically be obtained.

If we want to perform registration of images containing DWI data independently of a particular model and reconstruction method (such as the DT, dODF, fODF, ... from different reconstruction methods), it should be done *before* reconstruction, i.e. on the signal functions in q-space. This leads us to the problem of transforming these signal functions in q-space. In the literature, we found a method where the (local) affine transformation is simply applied straight to the gradient directions, whereafter they are normalized again [10]. Very recently, this approach showed up again [11]. While this works fine for a rigid rotation, we will show that it produces wrong results for affine transformations. We will also mention how this method can be easily fixed. However, this result is still not sufficient because volume fractions are not preserved. We will then start off from the method of Raffelt et al. [13]. Using the relations of Descoteaux et al. [5–7], we will translate this method back to the signals in q-space. We add upon this by including an isotropic volume fraction (IVF), so as to preserve its isotropic nature. As such, our new method is able to handle the transformation of full images (i.e. no threshold on anisotropy needed) containing DWI data in q-space while preserving anisotropic as well as isotropic volume fractions.

In the results section, we show the impact of (not) accounting for the IVF on quantitative measures that are also calculated straight on the signals in q-space. The qualitative impact on, for instance, reconstructed fODF's is also briefly discussed.

2 Methods

2.1 About reorienting the gradient directions

A very straightforward method to perform the (local) affine transformation can be found in the literature [10, 11]. It simply consists of applying the transformation to the gradient directions and normalizing the result so as to obtain a new

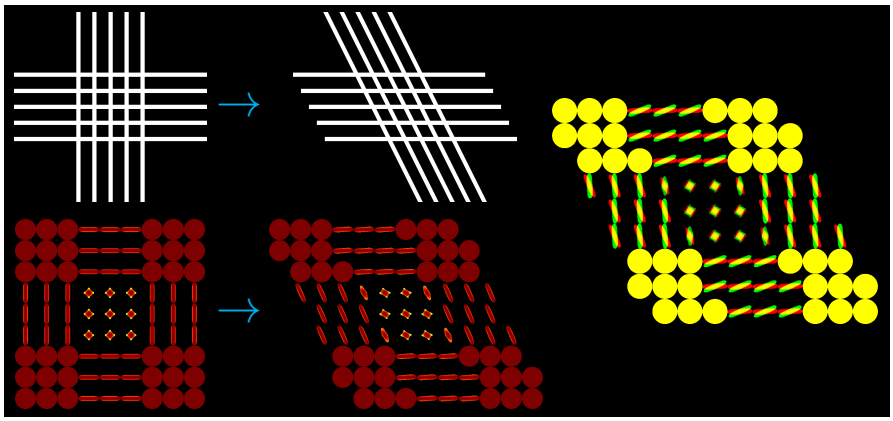

Fig. 1. A set of crossing fibers (*top left*) is being sheared (*top middle*). The sampling directions of the corresponding signal functions (*bottom left*) are sheared in the same way (*bottom middle*). The result is however highly inconsistent with the sheared fibers. This method (*red*) is overlaid with our fixed version (*green*) (*right*).

set of gradient directions for the voxel in question. In case of an affine transformation matrix M and gradient directions g, the new gradient directions g' can thus be found by $g' = Mg/\|Mg\|$. While it may intuitively seem a good idea to apply the transformation to the sampling directions of something like an fODF, this can however *not* be done in the same way to the signal functions to obtain a similar result! An example clarifies this statement. In Fig. 1, a small patch of crossing fibers is shown being sheared. This particular shearing changes the orientation of the vertical bundle, but leaves the orientation of the horizontal bundle unaffected. If we apply the same shearing to the sampling directions of the signal function (i.e. to the gradient directions), the outcome is highly inconsistent with the sheared fiber structure. The voxels in the vertical bundle barely changed, while the ones in the horizontal bundle were reoriented quite a lot.

After some reasoning, we could fix this method: the new gradient directions can actually be obtained by $g' = Ng/\|Ng\|$ instead, where the matrix N can be calculated as $N = (M^{\mathrm{T}})^{-1}$. A comparison of this fixed method and the original one is also presented in Fig. 1. We won't go into further details about this reasoning, as this result is still not satisfactionary: while it changes sampling directions, it does in no way preserve volume fractions.

2.2 Preserving volume fractions

Signals in q-space, the dODF and the fODF in a single voxel are angular functions, which can be represented by functions on the unit sphere. SH functions provide a basis for complex functions on the unit sphere. They are defined as

$$Y_\ell^m(\theta,\phi) = \sqrt{\frac{2\ell+1}{4\pi}\frac{(\ell-m)!}{(\ell+m)!}}P_\ell^m(\cos\theta)e^{im\phi} \tag{1}$$

where P_ℓ^m is an associated Legendre polynomial. The nonnegative integer ℓ denotes the order and the integer $m \in [-\ell, \ell]$ is a phase factor. Using only even orders ℓ, a new basis with index $j = (\ell^2 + \ell + 2)/2 + m$ can be constructed as

$$Y_j = \begin{cases} \sqrt{2} \cdot \mathrm{Re}(Y_\ell^m) & \text{if } -\ell \leq m < 0 \\ Y_\ell^0 & \text{if } m = 0 \\ \sqrt{2} \cdot \mathrm{Im}(Y_\ell^m) & \text{if } 0 < m \leq \ell \end{cases} \tag{2}$$

which consists of $T = (n+1)(n+2)/2$ terms, where n is the maximum order [5]. This basis has the useful properties of being real-valued, antipodally symmetric and orthonormal with respect to the inner product. We can now express the measured signal S for gradient direction (θ_i, ϕ_i) in a single voxel as a function

$$S(\theta_i, \phi_i) = \sum_{j=1}^{T} c_j Y_j(\theta_i, \phi_i) \tag{3}$$

of which the coefficients c_j can be estimated using a linear least-squares method while directly incorporating a local Laplace-Beltrami regularization [5].

The dODF can be estimated from the signal on a single sphere of q-space by the Funk-Radon transform (FRT), of which the value in direction u equals the integral over the corresponding equator [2]. Representing both S and the dODF in the SH basis allows for a simplification of the FRT given by

$$\mathrm{FRT}[S](u) = \int_{w \perp u} S(w) dw = \sum_{j=1}^{T} 2\pi P_{\ell_j}(0) c_j Y_j(u) = \sum_{j=1}^{T} c'_j Y_j(u) \tag{4}$$

where ℓ_j is the order of Y_j and P_{ℓ_j} is the Legendre polynomial of degree ℓ_j [6]. This means the coefficient vector C' of the dODF can be obtained through a linear transformation of the coefficient vector C of the signals by $C' = FC$ where F is a diagonal matrix.

In a similar manner, the fODF can be estimated from the dODF by the sharpening deconvolution transform (SDT), which is a SD of the dODF with the single fiber dODF kernel R' (shaped by the b-value and eigenvalues λ_1 and $\lambda_2 = \lambda_3$) [7]. A simplified analytical solution is now given by

$$\mathrm{SDT}[\mathrm{FRT}[S]](u) = \sum_{j=1}^{T} \frac{c'_j}{2\pi \int_{-1}^{1} P_{\ell_j}(t) R'(t) dt} Y_j(u) = \sum_{j=1}^{T} c''_j Y_j(u) \tag{5}$$

allowing for the calculation of the coefficient vector C'' of the fODF by $C'' = DC'$ where D is a diagonal matrix. An important property of both the FRT and the SDT is that they are linear and invertible within the context of our symmetric SH basis.

Raffelt et al. [13] start off from the fODF represented in a SH basis. They then approximate the fODF by a weighted sum of SH delta functions. Due to

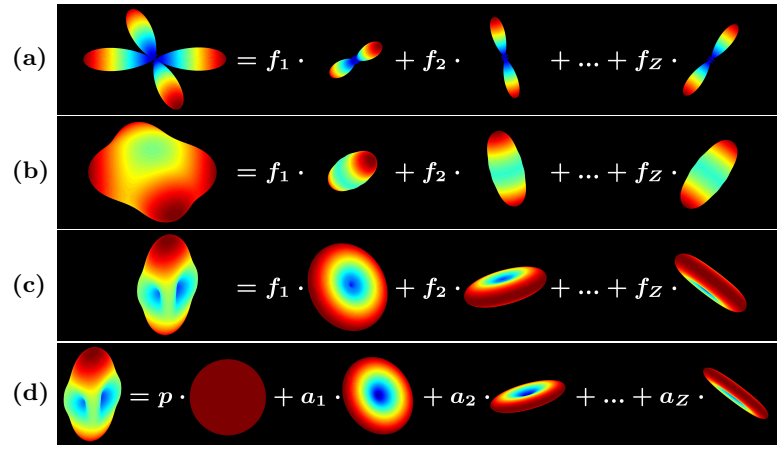

Fig. 2. Transformation-friendly representation **(a)** of the fODF, **(b)** of the dODF, **(c)** of S in q-space and **(d)** also accounting for isotropic volume fractions.

orthonormality of the SH basis, a delta function $\delta(\theta, \phi)$ can be projected into the elements of the coefficient vector E'' of a SH delta function by

$$e''_j = \int_\Omega \delta(\theta, \phi) Y_j(\theta, \phi) d\Omega \tag{6}$$

Denoting the SH delta function of maximum order n with its main axis along direction z by δ_n^z, the fODF can then be approximated as shown in Fig. 2a by

$$\mathrm{SDT}[\mathrm{FRT}[S]](u) = \sum_{i=1}^{Z} f_i \delta_n^{z_i}(u) \tag{7}$$

using $Z > T$ uniformly distributed directions z_i and obtaining the fractions f_i. An affine transformation of the fODF is then achieved by subjecting the directions z_i to this transformation, while maintaining the fractions f_i. This can in a way be seen as a natural extension of the PPD approach in DTI: each $f_i \delta_n^{z_i}$ is independently subjected to a rigid PPD (z_i) transformation. We will call a representation such as (7) a transformation-friendly representation (TFR).

Because the SDT and FRT are linear and invertible, we can rewrite (7) as

$$S(u) = \sum_{i=1}^{Z} f_i \, \mathrm{FRT}^{-1}[\mathrm{SDT}^{-1}[\delta_n^{z_i}]](u) = \sum_{i=1}^{Z} f_i \beta_n^{z_i}(u) \tag{8}$$

so as to obtain an equivalent TFR of S in q-space, as shown in Fig. 2c. The elements of the coefficient vector E of a SH β_n^z function can be calculated from E'' of a SH delta function by $E = (DF)^{-1}E''$. This TFR of S should theoretically have the same fractions f_i as TFR (7) of the fODF and subjecting either of both TFR's to any affine transformation should produce the same result.

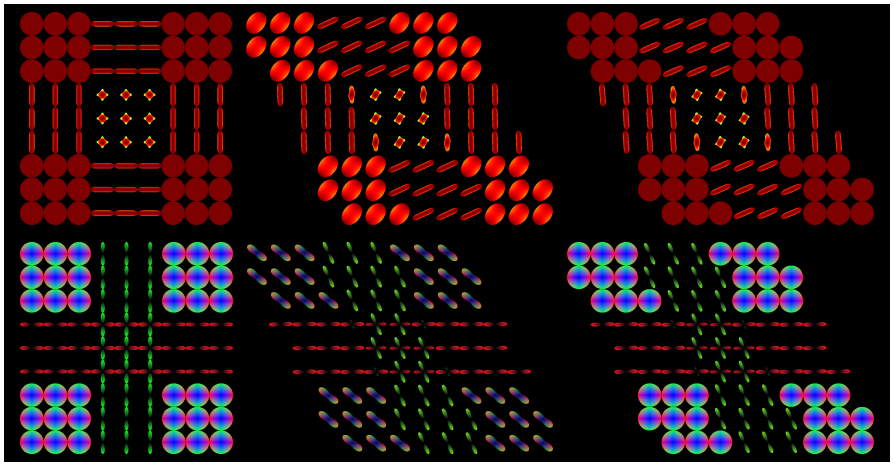

Fig. 3. The signal functions (*top left*) are sheared using TFR (8) (*top middle*). This however causes isotropic diffusion to become anisotropic. When using the new TFR (9), the problem is solved (*top right*). Corresponding fODF's calculated from the top row are also shown (*bottom row*).

However, examples can be found where the outcome will not satisfy. For instance, when shearing a voxel containing isotropic diffusion, we would like the outcome to still be isotropic, but this will not be the case due to the preservation of volume fractions. This example is also shown in Fig. 3. The problem is neither with the method nor the general idea of preserving volume fractions, but rather with the choice of fractions. We therefore suggest a new TFR of S as shown in Fig. 2d, which we define as

$$S(u) = pY_1 + \sum_{i=1}^{Z} a_i \alpha_n^{z_i}(u) \tag{9}$$

where the coefficient vector of a SH α_n^z function is $[0, e_2, e_3, ..., e_T]^{\mathrm{T}}$ (with e_2–e_T from the coefficient vector E of the corresponding SH β_n^z function). Because $Y_1 = Y_0^0$ is a constant function, we now obtain a single isotropic volume fraction (IVF) p and Z anisotropic volume fractions a_i. The result of using this new TFR in the case of the previous example can be seen in Fig. 3.

3 Results

We choose to focus on presenting a selection of results on the comparison of TFR (8) of S (Fig. 2c) – which is a translation of the method of Raffelt et al. [13] to q-space – and the new TFR (9) of S that accounts for IVF's (Fig. 2d).

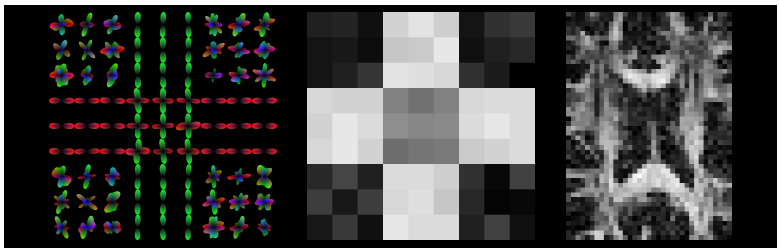

Fig. 4. The data: reconstructed fODF's (*left*) and GFA (*middle*) of the simulated data; GFA of the real data (*right*)

3.1 Data

Simulated data of a crossing was constructed for 75 gradient directions at $b = 3000s/mm^2$ using the multi-tensor model (anisotropic tensors with $\lambda_1 = 0.0018$ and $\lambda_2 = \lambda_3 = 0.0006$; isotropic tensors with $\lambda_1 = \lambda_2 = \lambda_3 = 0.0020$), after which Rician noise (SNR = 50) was added. Fig. 4 shows reconstructed fODF's from these data, as well as a generalized fractional anisotropy (GFA) image. GFA is calculated by

$$\mathrm{GFA}(S) = \frac{\mathrm{std}(S)}{\mathrm{rms}(S)} = \sqrt{1 - \frac{c_1^2}{\sum_{j=1}^{T} c_j^2}} \tag{10}$$

straight on the SH coefficients of a signal function S.

Real data were acquired from a single healthy subject on a Siemens 3T scanner, with a $2.5mm$ isotropic voxel size, 75 gradient directions at $b = 2800s/mm^2$ and 10 repetitions of $b = 0$ (averaged). Fig. 4 shows a GFA image of the patch for which results are presented.

For both datasets, the SH coefficients of S were calculated up to order 6. To account for the noise, Laplace-Beltrami regularization was applied. From the SH representations of S, we then calculated both TFR's (8) and (9) (assuming a single fiber dODF kernel R' shaped by $\lambda_1 = 0.0018$ and $\lambda_2 = \lambda_3 = 0.0003$ to obtain the coefficient vectors of the SH β_n^z and α_n^z functions), with $Z = 300$ uniformly distributed directions z_i (obtained through electrostatic repulsion). Using each of both TFR's, 2 transformations were applied (a shear $[1, 0.5, 0; 0, 1, 0; 0, 0, 1]$ and a stretch $[1.5, 0, 0; 0, 1, 0; 0, 0, 1]$), after which the SH coefficients of the transformed S were again calculated. These were then compared in different ways.

3.2 Angular similarity

To compare the angular similarity between 2 signal functions, an angular similarity measure can be obtained by normalizing both SH coefficient vectors ($C_a^{\mathrm{T}} C_a = C_b^{\mathrm{T}} C_b = 1$) and calculating the inner product $C_a^{\mathrm{T}} C_b$. It may as such vary between 0 and 1. We calculated this measure between the outcomes of using both TFR's. The results are shown in Fig. 5.

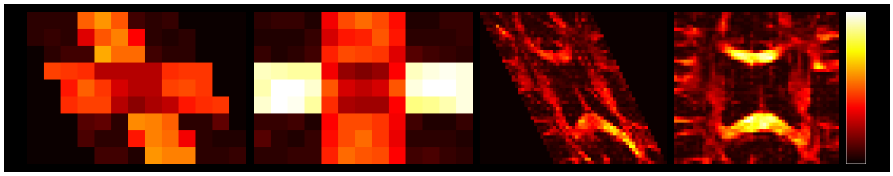

Fig. 5. Angular similarity after using both TFR's for the shearing and stretching of the simulated and real data. The color scale varies from 0.9966 (*dark*, less similar) to 0.9978 (*bright*, more similar).

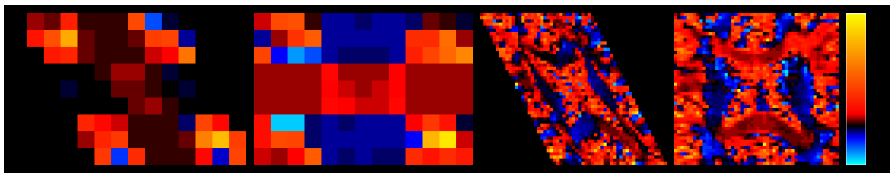

Fig. 6. Relative GFA difference after using both TFR's for the shearing and stretching of the simulated and real data. The color scale varies from 1/3 (*cyan*) over 1 (*black*) to 3 (*yellow*).

The first thing to notice is that the absolute values of the measure are very high. This makes sense, as the voxels compared should actually represent the same data, apart from the TFR used. Large differences in the angular structure itself are not expected. We are however interested in the relative difference between different tissue types: where does accounting for IVF's matter the most? The difference is clearly the largest in the more isotropic parts (this was also quite expected). However, the difference also seems to be dependent on the orientation of fibers relative to the transformation (this can most easily be seen in the stretching of the simulated data).

3.3 Relative GFA difference

GFA was calculated from the results of using TFR (8) and TFR (9) and relative GFA difference was defined as the division of the former (*not* accounting for IVF's) by the latter (accounting for IVF's). The results are shown in Fig. 6.

Not accounting for IVF's causes GFA to mostly go up in the isotropic parts. In the results of both simulated and real data, we also see that it is lowered in a few voxels of the isotropic parts. This can probably be attributed to specific interactions with the noise. In the other (more anisotropic) parts, the relative difference of GFA between both outcomes is clearly dependent on the specific combination of the local angular structure and the applied transformation: in some regions it goes up while in others it is lowered. The largest differences we could spot went up to a factor 3.

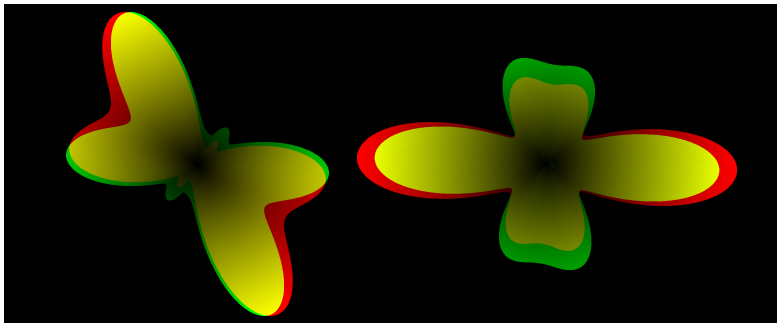

Fig. 7. Qualitative comparison after using both TFR's for the shearing and stretching of the simulated data. fODF's are calculated for a voxel in the crossing. The results after accounting (*green*) and not accounting for IVF's (*red*) are overlaid.

3.4 Qualitative assessment

We also performed qualitative assessment on the signal functions as well as on fODF's that were calculated from them. Due to the presence of IVF's in many (if not all) voxels, we could spot differences in all voxels, of which the amount and nature corresponded to the earlier quantitative findings. As a clear example, we picked out a voxel in the crossing of the simulated data and calculated its fODF after applying the shearing as well as the stretching with both TFR's. The results of accounting and not accounting for IVF's were overlaid for comparison of shape. The results are shown in Fig. 7.

Not accounting for IVF's caused the peaks to be less clearly separated in the case of the shearing. In the case of the stretching, we noticed that the peaks ended up with different relative sizes. It's clear that the difference between accounting and not accounting for IVF's in general can be seen in the end result as a difference in relative sizes between different volume fractions. In the case of a decreasing in angle between some peaks, an IVF that gets not accounted for (i.e. gets deformed) might cause peaks that are less clearly separated from each other than if the IVF would have been accounted for.

4 Discussion and Conclusion

In this work, we studied the problem of spatially transforming DWI data in q-space. Our main motivation is that it will enable us to perform registration on DWI data *before* the reconstruction of any particular model (a tensor, a dODF, a fODF, ... amongst others) while making maximum use of the information in the original data. We reasoned that the problem could be reduced to *affine transformation of the information in a single voxel*, because in the case of a non-rigid deformation field, the Jacobian matrix provides a local affine model for each voxel.

We started by looking into a simple method that is found in the literature [10, 11], which basically consists of applying the (local) affine transformation to

the gradient directions (and normalizing again) to obtain a new set of gradient directions. However, by use of a clear example, we showed that this method causes wrong results for affine transformations. The method could easily be fixed by not using the transformation matrix itself, but rather the inverse of its transpose, to reorient the gradient directions. This makes for a major difference in the end result. As the inverse of the transpose of a rigid rotation matrix equals again the original matrix, both the method and the fixed version give the same results for that specific case. We presume this fact to be the cause of why the issue could have been overlooked in the past.

But even this fixed method is not satisfactionary, because it only reorients sampling directions (i.e. the magnitude of the samples itself is unaffected) and as such does not preserve volume fractions. Using (reversing) the methods of Descoteaux et al. [5–7] and starting from the representation of the fODF by a sum of SH delta functions as introduced by Raffelt et al. [13], we have shown how affine transformation of the fODF with preservation of volume fractions can be translated to equivalent approaches for transforming the dODF and the signals S in q-space. These approaches can in a way be seen as a natural extension of PPD, because each of the components of a TFR (Fig. 2) is independently subjected to a rigid PPD transformation.

Again reasoning on a simple example, we found our newly translated TFR (8) (Fig. 2c) not yet able to deal correctly with the case of isotropic diffusion. Therefore, we defined a new TFR (9) (Fig. 2d) of S by including an IVF, while preventing the other (anisotropic) volume fractions to represent any isotropic part (Fig. 2d). Using this new TFR for affine transformation, the IVF in each voxel is automatically preserved (as well as all the anisotropic volume fractions are). The impact of improvement is proportional to the magnitude of the IVF (i.e. inversely proportional to an anisotropy measure). While accounting for IVF's mostly improves the outcome for the voxels containing less anisotropic tissue, it also has an impact on all other voxels in a real(istic) dataset, so just using an anisotropy mask doesn't avoid the problem.

Because one of the major motivations for doing image registration might be a quantitative voxel based analysis, it is of high importance that the information inside each voxel gets transformed in the most correct way possible. We have shown that not accounting for the IVF has a clear impact on, for instance, a GFA measure that is calculated from the end result. There were also differences in angular structure as well as qualitative differences. These differences might even grow more severe if specific reconstruction schemes are applied after registration.

As our method can naturally deal with all voxels, be they anywhere in the spectrum between isotropic and highly anisotropic, no anisotropy mask is needed during registration and the information in all voxels can be put to good use. The method is mostly suited for HARDI data that consist of one or more shells in q-space. Each shell containing enough samples can then be represented in a SH basis, whereafter the method can be performed on the different shells. While we are as such able to spatially transform the data before the reconstruction of any particular model of diffusion, our method does however depend on a suitable

choice of the single fiber kernel. Using the SDT [7], the assumption of a tensor model is made for the construction of the kernel. In practice, it is also possible to estimate the single fiber signal response function from the data itself [3, 4]. This response function can then be used as the β function for TFR (8) (Fig. 2c), and the α function for TFR (9) (Fig. 2d) is easily obtained from the β function in the same way as we explained before. Using the methods of Descoteaux et al. [5–7] provides an insight that transcends the representation of HARDI data.

Future work will focus on incorporating this new model for transforming S in q-space while accounting for IVF's in a coregistration algorithm, using the (angular) information in all voxels of the full brain volumes. This might then allow for better precision of the coregistration outcome, more reliable voxel-based analyses or the construction of a high quality full brain HARDI (q-space) atlas.

References

1. Tuch, D.S., Reese, T.G., Wiegell, M.R., Makris, N., Belliveau, J.W., Wedeen, V.J.: High Angular Resolution Diffusion Imaging Reveals Intravoxel White Matter Fiber Heterogeneity. MRM 48(4), 577–582 (2002)
2. Tuch, D.S.: Q-Ball Imaging. MRM 52(6), 1358–1372 (2004)
3. Tournier, J.D., Calamante, F., Gadian, D.G., Connelly, A.: Direct Estimation of the Fiber Orientation Density Function from Diffusion-Weighted MRI Data using Spherical Deconvolution. NeuroImage 23(3), 1176–1185 (2004)
4. Tournier, J.D., Calamante, F., Connelly, A.: Robust Determination of the Fibre Orientation Distribution in Diffusion MRI: Non-negativity Constrained Super-resolved Spherical Deconvolution. NeuroImage 35(4), 1459–1472 (2007)
5. Descoteaux, M., Angelino, E., Fitzgibbons, S., Deriche, R.: Apparent Diffusion Coefficients from High Angular Resolution Diffusion Imaging: Estimation and Applications. MRM 56(2), 395–410 (2006)
6. Descoteaux, M., Angelino, E., Fitzgibbons, S., Deriche, R.: Regularized, Fast, and Robust Analytical Q-Ball Imaging. MRM 58(3), 497–510 (2007)
7. Descoteaux, M., Deriche, R., Knösche, T.R., Anwander, A.: Deterministic and Probabilistic Tractography based on Complex Fibre Orientation Distributions. IEEE TMI 28(2), 269–286 (2009)
8. Alexander, D.C., Pierpaoli, C., Basser, P.J., Gee, J.C.: Spatial Transformations of Diffusion Tensor Magnetic Resonance Images. IEEE TMI 20(11), 1131–1139 (2001)
9. Barmpoutis, A., Vemuri, B.C., Forder, J.R.: Registration of High Angular Resolution Diffusion MRI Images using 4^{th} Order Tensors. MICCAI 10(1), 908–915 (2007)
10. Tao, X., Miller, J.V.: A Method for Registering Diffusion Weighted Magnetic Resonance Images. MICCAI 9(2), 594–602 (2006)
11. Yap, P.T., Chen, Y., An, H., Gilmore, J.H., Lin, W., Shen, D.: Non-Parametric Deformable Registration of High Angular Resolution Diffusion Data using Diffusion Profile Statistics. ISMRM 18, 3968 (2010)
12. Hong, X., Arlinghaus, L.R., Anderson, A.W.: Spatial Normalization of the Fiber Orientation Distribution Based on High Angular Resolution Diffusion Imaging. MRM 61(6), 1520–1527 (2009)
13. Raffelt, D., Tournier, J.D., Fripp, J., Crozier, S., Connelly, A., Salvado, O.: Non-Linear Spatial Normalization of High Angular Resolution Diffusion Imaging Data using Fiber Orientation Distributions. MICCAI 12, DMFC Workshop (2009)